



Seismic response across the Tronto Valley (at Acquasanta Terme, AP, Marche) based on the geophysical monitoring of the 2016 Central Italy seismic sequence

Antonio Costanzo¹ · Arrigo Caserta²

Received: 11 September 2018 / Accepted: 22 March 2019 / Published online: 12 April 2019
© Springer-Verlag GmbH Germany, part of Springer Nature 2019

Abstract

Since August 2016, Central Italy has been struck by three strong earthquakes (Mw 6.0 Amatrice, Mw 5.9 Visso and Mw 6.5 Norcia). This seismic sequence resulted in ground failure, infrastructural damages and destruction of several villages. This work aims to analyze the site effects on the ground shaking along the valley of the Tronto River across the Acquasanta Terme municipality, where some historical sites were located. These suffered heavy and differentiated damage during the seismic sequence. Following the Amatrice earthquake of August 24, authors managed the deployment and acquisition of seismic stations located in an array along the valley of the Tronto River approximately 25 km from the epicenter. By recording the two stronger earthquakes (i.e., Mw 5.9 Visso and Mw 6.5 Norcia) and 30 aftershocks with varying magnitudes and also ambient vibration, the site effects were preliminarily studied using the horizontal-to-vertical spectral ratio (HVSr). Furthermore, the amplification effects on the ground motion were also evaluated with reference to the earthquakes in terms of the standard spectral ratio (SSR) and the normalized energy content, in both cases using the bottom of the valley where the seismic bedrock outcrops as a reference. The comparison between the spectral accelerations due to the two strong earthquakes and those provided by ground motion prediction equations displayed values that were usually inadequately precautionary for periods lower than 0.35 s. High spectral accelerations were detected in period ranges corresponding to those predominant for masonry structures that are available in the literature. According to the current knowledge about surface geology, the local site effects seem to have significantly influenced ground shaking along the slopes of the valley, thus producing a larger seismic effect on ancient structures with more than two floors. The results can provide useful information for undertaking a possible future microzonation study that would be able to support urban planning and seismic designs in the rebuilding phase.

Keywords Seismic response · Tronto Valley · Site effects · Geophysical monitoring · Central Italy seismic sequence · Ground motion prediction equations

Introduction

On August 24, 2016, a Mw 6.0 earthquake struck an extended region of the Central Apennines, one of the most seismically active areas in Italy. This devastating earthquake (see red star in Fig. 1a) occurred close to the village of Accumoli (epicentral distance of about 1 km) and the town of Amatrice

(epicentral distance 10 km), causing 299 casualties and severe damage to buildings (Masi et al. 2017; Fiorentino et al. 2018) and historic heritage (Caserta et al. 2016) in several towns surrounding the epicenter. The following seismic sequence produced hundreds of aftershocks for the following days (Michele et al. 2016), including a Mw 5.4 earthquake on the same day. Approximately 2 mo after the Amatrice earthquake, on October 26, two other severe earthquakes (Mw 5.4 and 5.9) occurred about 14 km NNE of Norcia near the village of Visso. These earthquakes preceded the strongest event of the sequence—an earthquake of Mw 6.5 that occurred on October 30 (at 06:40:18 UTC) about 5 km North of Norcia (Fig. 1).

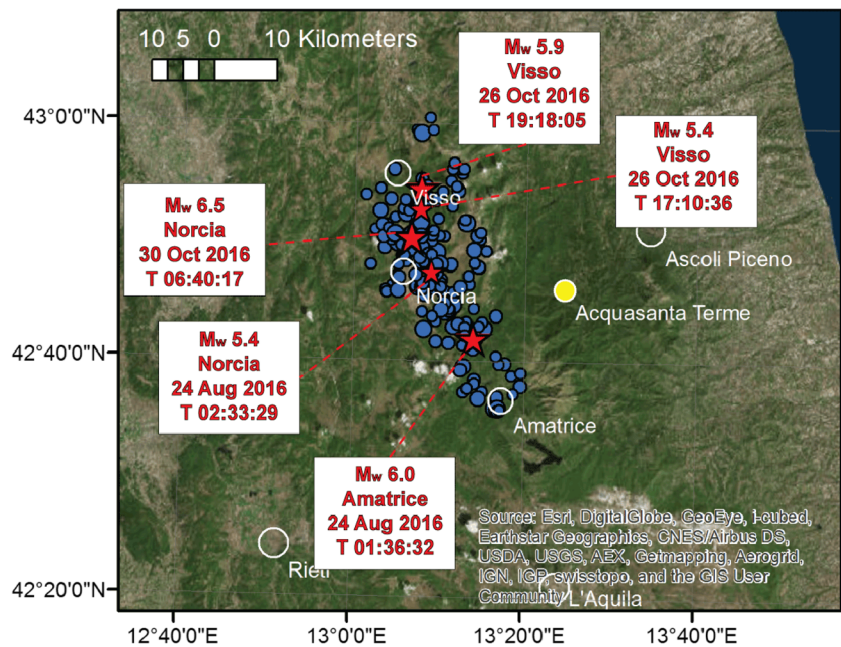
Immediately after the beginning of the seismic sequence, the Emersito operative group coordinated the monitoring of the local site effects and installed a temporary seismic network

✉ Antonio Costanzo
antonio.costanzo@ingv.it

¹ Istituto Nazionale di Geofisica e Vulcanologia, Via P. Bucci, Cubo 30/C - piano 7, Rende (CS) 87036, Italy

² Istituto Nazionale di Geofisica e Vulcanologia, Via di Vigna Murata 605, Rome 00143, Italy

Fig. 1 Epicentres (blue circles) of the August–October 2016 seismic sequence in the central Apennine mountain chain. The epicenters of stronger earthquakes (red stars) are located between 16 and 28 km from Acquisanta Terme (yellow circle)



in the epicentral area. The preliminary analysis showed the lengthening and amplification of the seismograms and variability of the peaked frequency related to the thickness of the sedimentary deposits in the basin between Montereale e Capitignano, about 18 km south of the epicenter of the Amatrice earthquake (Cultrera et al. 2016). Data analysis from 20 years of seismic monitoring (Pilz and Parolai 2009) allowed the detection of resonance frequencies dependent on the sediment depth in the Norcia intermountain basin (Luzi et al. 2018), as well where the historic town of the same name is located; the town suffered severe damage during the seismic sequence (Galli et al. 2017).

Masi et al. (2016) discovered different levels of damage in two villages in the Arquata del Tronto municipality; the first one suffered the collapse of several buildings (i.e., Pescara del Tronto located about 6.5 km NNE of the epicenter of the Amatrice earthquake) while the other witnessed light damage to a few buildings (i.e., Vezzano), despite the two villages being separated by only 1300 m. This unexpected anomaly regarding damage distribution was verified through the site response as observed in the geophysical investigation performed. Other geophysical studies were conducted immediately after the destructive seismic sequence in order to collect information for possible studies of microzonation and for providing information for reconstruction planning. Evaluations of the local seismic responses based on the seismological data were performed for different sites in the areas more damaged by the central Italy seismic sequence (e.g., Laurenzano et al. 2018) in order to support the microzonation studies commissioned by the Italian Civil Protection Department.

Following the Amatrice earthquake, the authors joined the group that was designated by Emersito for monitoring in the

Acquisanta Terme municipality that lies 25–30 km away from the epicenters of the three main events. This municipality comprises several historical settlements located along the slopes of the river, which are composed predominantly of residential masonry buildings and some reinforced concrete structures (e.g., accommodation facilities and a school). Several of these buildings suffered a significant grade of damage because of the shaking produced by the first seismic event (i.e., Mw 6.0 Amatrice earthquake). Diffuse damages were detected both on the masonry and the reinforced concrete structures by conducting visual inspections of the observed effects. Several of these buildings were subsequently identified as inhabitable after surveys by competent authorities. Nevertheless, the damage grade seemed to display an overall increase from the valley bottom towards the settlements located along the flanks of the river. Therefore, we decided to investigate site effects along the cross-section that intersected the settlements of the town. In early September 2016, we deployed a seismic array along the valley of the Tronto River (red triangles in Fig. 2) crossing the town of Acquisanta Terme at about 25 km from the epicenter (yellow circle Fig. 1) as part of this framework. Continuous geophysical monitoring allowed the recording of the seismic sequence that aggravated the damage.

This work aims to analyze whether amplification phenomena could have significantly impacted the ground shaking at the sites and seeks to quantify the seismic actions due to the stronger events. The data analysis also allows the drawing of some indications about the use of the spectral ratios most commonly used in practice. Initially, the paper discusses the similarities and differences detected on the recordings of the Mw 5.9 Visso earthquake and Mw 6.5 Norcia earthquake

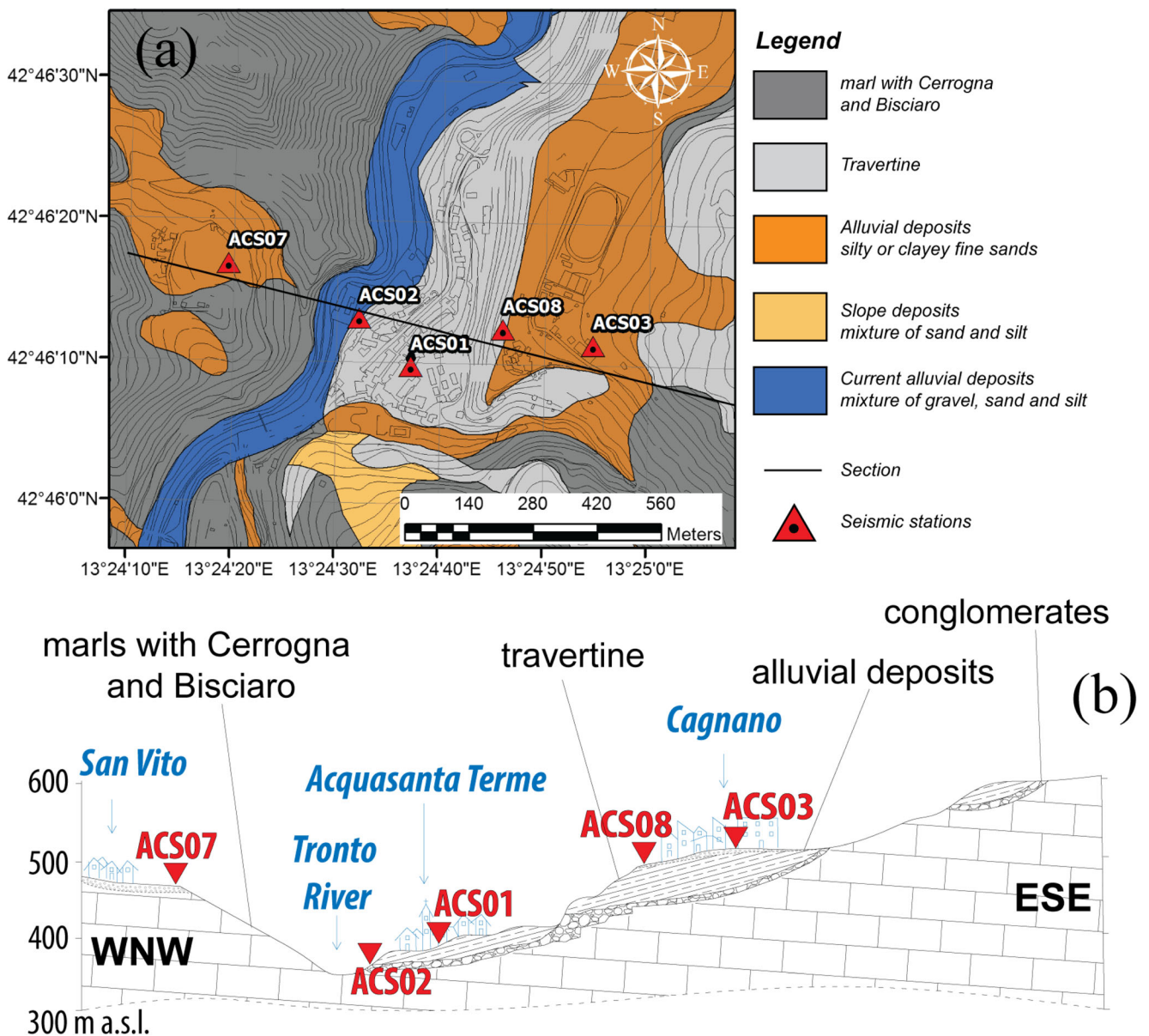


Fig. 2 Geological setting: (a) map of the study area and locations of seismic stations (red triangles); (b) schematic section along the Tronto Valley in correspondence of Acquasanta Terme (modified after Boni e

Colacicchi, 1966), with the seismic stations projected and the main settlements sketched on the same section

concerning the five sites along the cross-section of the Tronto Valley. Following this, the local effects were analyzed in terms of their spectral ratios by comparing those obtained from the recordings of the two strong earthquakes, 30 severe-to-moderate aftershocks and the ambient vibration. The spectral accelerations and energy content measured for the two strong earthquakes are compared with those provided by some ground motion prediction equations (GMPEs) available in the literature, which are obtained by studying datasets of the earthquakes that occurred in the Italian region as well as worldwide. Moreover, the spectral accelerations at different sites were superimposed on the predominant periods for

masonry buildings as available in the literature and correlated to the height of the structures. Finally, the conclusions are outlined.

Geological setting and recordings of the Central Italy seismic sequence

The town of Acquasanta Terme is located on the eastern side of the Tronto River. The municipality houses a town center and several hamlets on both sides of the valley. In this area, a large plate of travertine dominates the right flank of the Tronto

River related to the rise of sulfidic water (Boni and Colacicchi, 1966) or the revegetation at the beginning of interglacials (Farabollini et al., 2001). Along the right side of the valley, the travertine formation produces some terraces. Furthermore, continental deposits form thin covers composed of alluvial and detrital soils. Boni and Colacicchi (1966) also indicate the presence of some terraced deposits composed of sand and gravel that stay underneath the travertine formation. However, in the area of Acquasanta Terme they are not encountered by drillings that indicate travertine directly resting on the Miocene marly unit (cf. Lanzi and Cavanazza 1993; Prezzavento 2007). These latter formations, which include Bisciario, marl with Cerrognola and Pteropodi marl, are characterized by a thickness that can exceed 500 m and, together with the underlying Oligocene Scaglia Cinerea unit (up to 200 m thick), constitute the most important regional aquiclude (Galdenzi et al. 2010).

In summary, the settlements on the right flank of the Tronto River are located on terraces composed by travertine with an overlying layer of alluvial deposit. The deposit is generally composed of silty and clayey fine sands and characterized by thickness from a few meters, as in the town center, up to some tens of meters. The terraces rest on the Bisciario unit, which is considered a seismic bedrock (characterized by shear wave velocity $V_s > 1800$ m/s according to geophysical surveys carried out in the area for civil construction—cf. GEA 2007). Contrarily, the San Vito hamlet on the left flank of the valley rests on alluvial deposits directly overlying the same Miocene formation (Fig. 2a).

Since early September 2016, i.e., right after the Amatrice earthquake (August 24) and until May 2017, a seismic array was deployed along the section of the valley that crosses some settlements of the Acquasanta Terme municipality. Each seismic station was composed of a Centaur seismic digitizer (Nanometrics 2018a) equipped with a triaxial Trillium broadband seismometer (Nanometrics 2018b) and a triaxial Titan accelerometric transducer (Nanometrics 2018c). The horizontal components were oriented along the north-south and east-west directions. Data were continuously recorded and sampled at 250 Hz using 24-bit analog-to-digital converters. The time synchronism was provided by the embedded GPS at each station. A local wireless (WiFi) network was installed for data transmission—implemented by a set of antennas connected to each station and a server hosted in the municipal seat of the town. The temporary seismic stations were deployed along the WNW-ESE direction (cf. Table 1, map in Fig. 2a and section in Fig. 2b) as follows: the San Vito hamlet (station ACS07 at WNW), the thermal area at the bottom of the valley (ACS02), the town center of Acquasanta Terme (ACS01) and the lower (ACS08) and upper parts (ACS03 at ESE) of the village of Cagnano. The array was designed to investigate the role played by near-surface geology in amplifying soil shaking and to check the presence of any topographic effects.

In this work, recordings relative to the two stronger earthquakes (M_w 6.5 Norcia and M_w 5.9 Visso) were analyzed, including thirty aftershocks with variable magnitudes (between 5.4 and 3.0). Table 2 provides the date, time, location, depth and magnitude of the earthquakes examined. Furthermore, the epicentral distance (between 14 km and 33 km) and site-to-epicenter azimuth (between 223° and 317°) are provided with reference to the town center of Acquasanta Terme.

The smoothed Fourier amplitude spectra (FAS) obtained from the recordings of the two stronger earthquakes are displayed for the five sites in Fig. 3. The horizontal motions from which the FAS were computed have been rotated into radial (R) and transverse (T) directions using a site-to-epicenter azimuth of 252° and 235° , respectively, for the Norcia and Visso earthquakes. The figure shows that the spectra have quite similar shapes for all the sites up to a frequency of approximately 1.5 Hz. The peaks of the FAS are between 20 Hz and 30 Hz at the valley bottom (ACS02 site) for the horizontal and vertical components, whereas these disappear at the other sites. On the right flank of the valley (ACS01, ACS08 and ACS03), the FAS exhibit maximum values almost always in the frequency range of 3–7 Hz for the horizontal components, with an increasing amplitude moving towards the ESE direction (cf. map in Fig. 2a and section in Fig. 2b). Nevertheless, another pronounced peak is detectable at high frequencies (>15 Hz) on the curves that referred to the ACS03 site. On the left bank of the valley (ACS07 site), finally, the maximum amplitudes of the FAS are observed in a wide range of frequency (3–15 Hz) without well-defined peaks in the transverse direction, depending on the examined event for the radial components (i.e., at approximately 3.5 Hz for the Norcia earthquake and 5.5 Hz for the Visso earthquake).

Site effects on the spectral response

The frequencies of the resonant peaks can be reliably detected using the horizontal-to-vertical spectral ratio (HVSr) (Lermo and Chávez-García 1993; Konno and Ohmachi 1998; Fäh et al. 2001; Bonnefoy-Claudet et al. 2006), especially for sites with a large impedance contrast in layers not far from the surface (up to hundreds of meters, depending on the value of the impedance contrast). According to Nakamura (2000), the H/V spectra can be controlled by the resonant effect due to the pathway of the SH-waves along the structure. Despite the observation that the H/V curve is useful to define fundamental frequency (Nakamura 2000), the shape and amplitude of the spectral ratio are not considered a good representation of the transfer function (Haghshenas et al. 2008). Since the H/V ratio could be related to the integrated contributions from different types of body waves and surface waves, the maximum values in the H/V spectra have to be carefully considered for estimating the SH-wave frequency of resonance.

Table 1 Details of the temporary network

COD	Station name	Latitude	Longitude	Elev. (m)	Start	Stop
ACS01	Terme	42.769	13.410	416	2016-09-01	2017-03-16
ACS02	Acquasanta	47.770	13.409	380	2016-09-01	2016-12-31
ACS03	Cagnano Up	42.770	13.415	506	2016-09-02	2016-11-14
ACS07	San Vito	42.771	13.406	449	2016-09-05	2016-11-23
ACS08	Cagnano Lo	42,770	13.412	465	2016-09-03	2017-03-16

In Fig. 4, the horizontal-to-vertical spectral ratios that referred both to the ambient vibrations (HVNSR) and the mean of the 30 earthquakes in Table 2 (HVSR) are compared. The confidence ranges are depicted by the shadowed area for noise

and dashed lines for earthquakes. Moreover, the HVSRs of the two earthquakes with higher magnitudes are recorded in the same figure. The HVSRs in the figure refer to the transverse (upper row) and longitudinal (lower row) components,

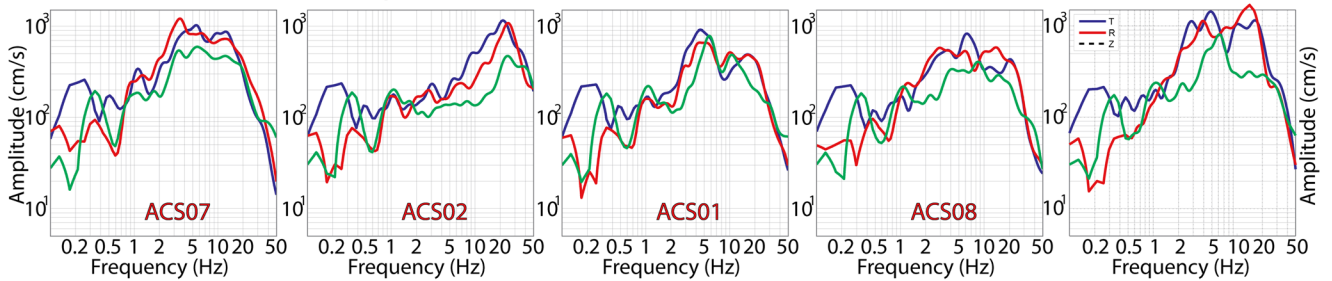
Table 2 Date and source parameters of earthquakes analyzed

Date	UTC Time	Latitude	Longitude	Depth/ Km	Magnitude ¹	Azimuth ² °]	Distance [km]
2016-10-30	06:40:17	42.840	13.110	9.4	6.5*	252.12	25.68
2016-10-26	19:18:06	42.9152	13.1278	8.4	5.9*	234.72	28.14
2016-10-26	17:10:36	42.8788	13.1287	9.3	5.4*	241.95	25.95
2016-10-26	21:42:02	42.8612	13.1283	9.5	4.5*	245.94	25.12
2016-10-27	03:50:24	42.9862	13.1268	8.9	4.4 ⁺	223.65	33.37
2016-10-27	08:21:46	42.8733	13.0998	9.3	4.3*	245.36	27.79
2016-10-27	17:22:23	42.841	13.1002	8.6	4.2*	252.42	26.47
2016-10-27	03:19:27	42.8442	13.1503	9	4.0*	248.45	22.74
2016-10-16	09:32:35	42.7542	13.1767	9.6	4.0*	274.99	19.08
2016-10-27	17:23:43	42.846	13.1085	8.4	3.9 ⁺	250.80	26.00
2016-10-26	19:25:19	42.9357	13.0747	8.5	3.9 ⁺	235.83	32.99
2016-10-08	18:11:10	42.7433	13.1927	10.9	3.9 ⁺	279.21	17.93
2016-10-26	19:43:44	42.8932	13.0693	9.8	3.8 ⁺	243.55	30.99
2016-10-28	13:56:33	42.8647	13.2142	5.1	3.7 ⁺	236.28	19.15
2016-10-26	21:24:52	42.8673	13.0783	9	3.7 ⁺	247.99	29.14
2016-10-27	07:50:30	42.8268	13.1343	9.1	3.6 ⁺	254.05	23.35
2016-10-27	02:44:46	42.9083	13.049	10.7	3.6 ⁺	242.23	33.22
2016-10-09	04:42:42	42.7437	13.1953	9.5	3.6 ⁺	279.18	17.71
2016-10-08	12:19:03	42.7502	13.1823	8.7	3.5 ⁺	276.47	18.67
2016-10-04	12:41:35	42.8545	13.121	7.8	3.4 ⁺	248.02	25.38
2016-10-02	23:47:07	42.7897	13.2303	9.4	3.4 ⁺	261.10	14.80
2016-09-30	19:38:38	42.8948	13.2468	9.3	3.4 ⁺	223.50	19.27
2016-09-30	19:22:28	42.896	13.2482	9.3	3.3 ⁺	317.02	19.29
2016-09-22	20:04:55	42.7597	13.1882	11.1	3.3 ⁺	266.68	18.10
2016-10-11	21:24:10	42.8672	13.0747	8.2	3.2 ⁺	291.78	29.41
2016-10-08	12:40:59	42.7508	13.1932	10.7	3.2 ⁺	263.42	17.78
2016-10-08	08:15:02	42.7802	13.2003	10.2	3.2 ⁺	274.13	17.12
2016-10-06	05:34:18	42.7935	13.2173	9.7	3.2 ⁺	279.81	15.92
2016-09-20	01:20:53	42.6772	13.2902	9.3	3.2 ⁺	223.62	14.12
2016-10-09	02:47:29	42.7442	13.1948	10.2	3.1 ⁺	261.02	17.75
2016-10-11	07:32:51	42.8562	13.2533	8.5	3.0 ⁺	307.25	16.00
2016-10-06	16:09:44	42.8793	13.1408	9.4	3.0 ⁺	299.22	25.11

¹ *Represents the moment magnitude (Mw) and ⁺ the local magnitude (MI)

² Site-to epicenter azimuth, clockwise from north

#1 - 2016.X.30 Norcia earthquake Mw=6.5



#2 - 2016.X.26 Visso earthquake Mw=5.9

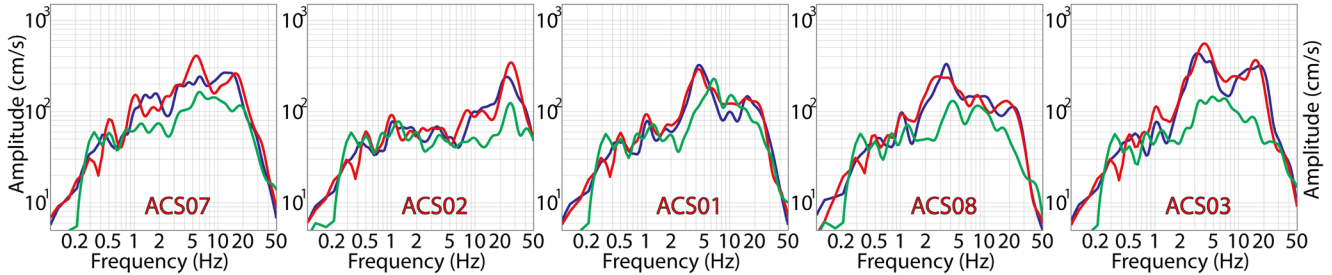


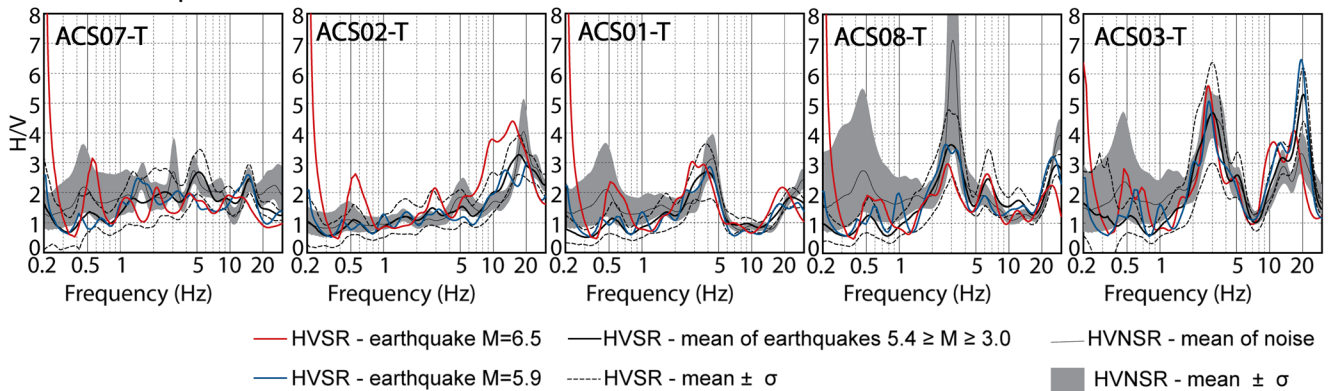
Fig. 3 Fourier Amplitude Spectra (FAS), smoothed using Konno and Ohmachi (1998) smoothing over logarithmic frequency, with their smoothing parameter set to $b = 20$. The spectra were computed from unfiltered acceleration time series

whereas the HVNSR is the geometrical mean of the two horizontal components.

The signal processing (same for all the recordings considered in the paper) included both the offset and mean removal and the application of an acausal 4-pole

Butterworth band-pass filter in the range of 0.1–25 Hz. The spectra were finally smoothed using the Konno and Ohmachi (1998) function with a smoothing coefficient equal to 20. Time histories were manually windowed to select S waves on the recordings of the earthquakes and

Transverse components



Radial components

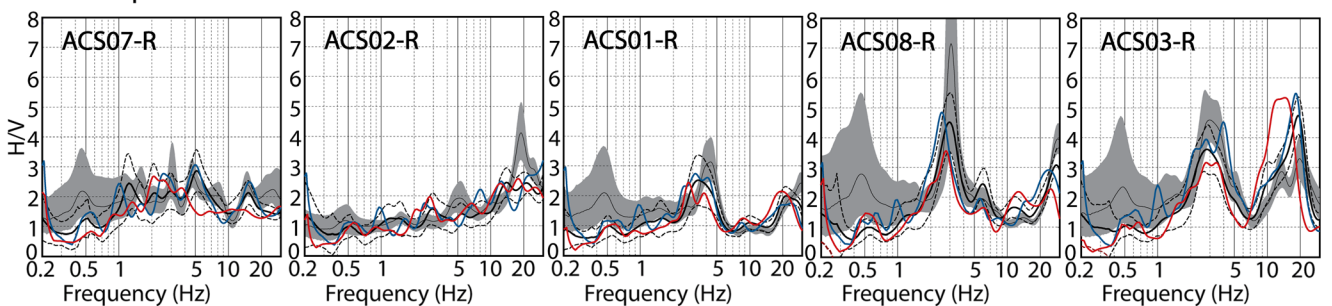


Fig. 4 Horizontal-to-vertical spectral ratios of the Fourier spectra, with comparison among ambient vibration, mean of 30 earthquakes ($5.4 \geq M \geq 3.0$), Mw 5.9 Visso earthquake and Mw 6.5 Norcia earthquake.

The horizontal motions for the earthquakes were rotated using the site-to-epicentre azimuth in Table 2, obtaining transverse (upper panel) and radial (lower panel) components

a 30 s window was adopted on 2-h recordings for ambient vibration.

The ratios obtained by noise and earthquakes exhibit good agreement in general, with the exception of those for low frequencies (< 1 Hz), where only the HVSNRs display a peak at approximately 0.5 Hz; however, it is characterized by high values of standard deviation.

Taking into account the frequencies with the value of HVSR higher than two as required by the clarity criterion specified by SESAME (2004), the following observations can be made:

- At the ACS02 site, the ratios highlight a resonance frequency between 18 Hz and 20 Hz by both noise and earthquakes; this is more pronounced for the latter ones by the transverse components, whereas the stronger earthquakes show a peak that shifted towards the lower frequencies.
- On the right bank of the Tronto Valley (ACS01, ACS08 and ACS03 sites), amplification is detectable in a range of frequencies between 2 Hz to 5 Hz, with a peak at around 4 Hz at ACS01 and approximately 3 Hz at ACS08 and ACS03.
- On the left bank of the valley, a resonance frequency cannot be clearly defined due to low statistical confidence. However, it should be noted that the 5 Hz amplitude assumes mean values of 2.5, with both noise and earthquakes, despite the stronger ones not highlighting the same behavior.

The H/V amplitudes in Fig. 4, generally, do not exceed the factor three, which could be considered as a reliable threshold for identifying the amplification frequencies.

Maps of the HVSR are shown as a function of azimuth and frequency to provide more information about directional effects due to morphological setting and types of motion (Fig. 5). The ratios obtained by ambient vibration, aftershocks and the two stronger earthquakes are compared. The two horizontal motions recorded at the same station were rotated into a specific azimuth to plot these graphs. Subsequently, the HVSR for this rotating motion was calculated. The procedure was repeated with azimuth steps of 10° starting from 0° N to 180° N counterclockwise, and thus the shaded contour map was constructed.

At the valley bottom, both the noise and the aftershocks allow the detection of amplification at high frequencies (around 19 Hz) with maximum values for azimuth between 130° – 170° N (Fig. 5a,b—ACS02), whereas the site shows a more complex behavior with significant amplification for frequencies greater than 10 Hz (Fig. 5c,d—ACS02) in the case of the two stronger earthquakes.

In the town center of Acquasanta Terme, the resonance frequency of 4 Hz is clearly shown by noise and aftershocks for all the azimuth directions (Fig. 5a,b—ACS01). Additionally, the ratio for the higher magnitude earthquakes shows amplification in the frequency range of 2.5–4.5 Hz (Fig. 5c,d—ACS01), with a polarization that remains fairly

consistent on the entire range. Nevertheless, the maximum values of the ratio are detectable, practically, on the entire azimuth range by ambient vibration, between $\pm 60^\circ$ N by aftershocks and about $\pm 50^\circ$ N by the Norcia and Visso earthquakes.

On the right side of the river at the two sites of the Cagnano village, the HVSR consistently allows the identification of amplification at a frequency around 3 Hz for all azimuth angles (Fig. 5a–d—ACS03 and ACS08). Furthermore, the HVNSR in the upper part of the village (i.e., ACS03) also gives relevant amplification values at high frequencies with peaks at approximately 12 Hz and 20 Hz continuous in the azimuth range, which is well distinguishable by noise (Fig. 5a—ACS03).

Finally, on the left side of the valley—close to the hamlet of San Vito—the ratios show peaks that are significantly dependent on the type of motion (Fig. 5a–d—ACS07). The amplification frequency of 5 Hz can be detected by all events except for the Norcia earthquake, in particular for azimuth angles between 0° N and 80° N.

In summary, the figure shows a general agreement between the different energy contents in identifying the first fundamental frequency. Furthermore, a polarization common to all sites (e.g., in perpendicular direction to the main elongation of the slope) does not seem identifiable.

In order to quantify the amplification factor, the standard spectral ratio (SSR) (Borcherdt 1970) was calculated as the ratio between the Fourier amplitude spectrum at the site and that at the reference site obtained for the same earthquake and the same component. For this purpose, the valley bottom (i.e., ACS02) was used as the reference; this site is at the contact between the travertine and Laga formations (Bisciario and Marls with Cerroigna, which was assumed as a seismic bedrock) and, as noted above, amplification effects are at a frequency of 19 Hz (cf. HVNSR in Figs. 4 and 5). In Fig. 6, the SSRs as the mean of the aftershocks and those that referred to two stronger earthquakes are reported for all sites and the three components of motion.

The SSR allows the identification of the amplification peaks and quantification of their values. Horizontal amplifications between 4 and 6 have been obtained by all motions around 4.5 Hz at the town center of Acquasanta Terme (ACS01), which substantially confirms the findings previously shown. At the two sites of Cagnano (ACS08 and ACS03), the horizontal ratios are greater in the frequency range between 2 Hz and 7 Hz. Nevertheless, the primary difference between these two sites lies in the different maximum values; the ratio obtained by recordings in the upper part of the village is almost double (with implies an SSR up to 8) with respect to the lower one. In the ACS03 site, amplification can also be observed at higher frequencies (> 10 Hz); however, its values are significantly lower than the previous ones. On the left bank of the river (ACS07), for aftershocks, the peak of the amplification ratio is well detectable around 6 Hz with a mean value higher than 9. It is worth emphasizing that the SSRs are

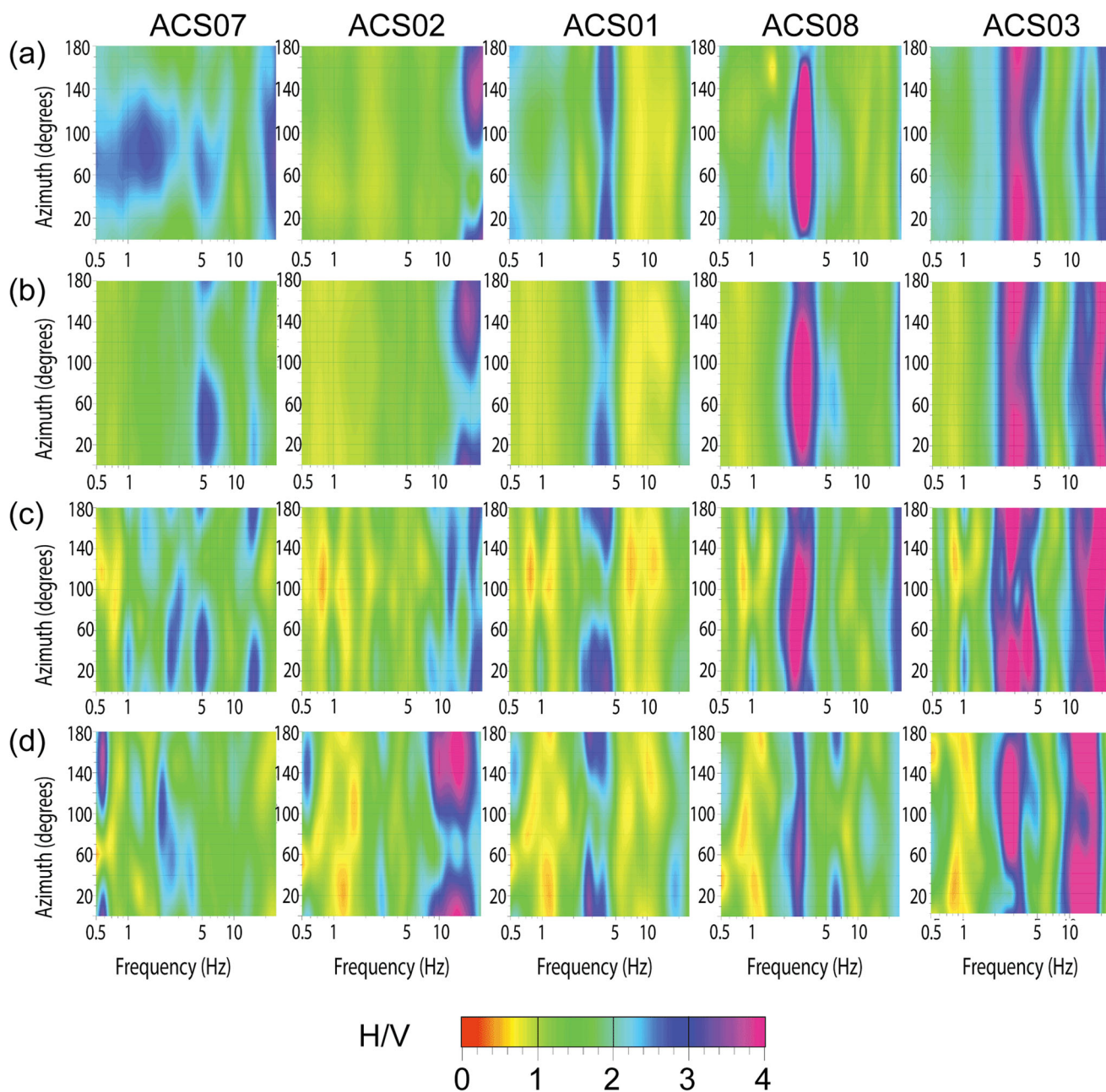


Fig. 5 Maps of the horizontal-to-vertical (H/V) spectral ratios of the Fourier spectra as a function of the azimuth angle and frequency, with comparison among ambient vibrations (a), mean of thirty aftershocks (b), Mw 5.9 Visso earthquake (c) and Mw 6.5 Norcia earthquake (d). The

horizontal components were obtained by rotating the observed components into the azimuth shown on the ordinate scale (0 degrees correspond to the North)

affected by the non-flat response above 15 Hz at the reference site (especially in the transverse component). Therefore, the ratios are not reliable above this frequency value. In summary, a significant amplification is encountered for all sites with respect to the valley bottom in variable frequency ranges that generally contain the frequencies of the HVSr peaks.

In addition, Fig. 6 shows a probable effect related to the non-linear behavior of the soils, especially at the ACS03 and ACS07 sites. A decrease in the peak amplitudes and their frequencies

seems to correspond with the increase of the energy content. It is noteworthy that these sites are characterized by outcropping layers of deformable silty-clayey deposit with a thickness of some tens of meters, superimposed on a stiffer formation (i.e., the travertine for ACS03 or, directly, the base marls for ACS07).

With reference to the vertical components (lower row in Fig. 6) and despite the maximum amplitudes of the ratio being comparable, the SSR curves are characterized by an amplification peak of around 6 Hz and more or less narrow shape,

depending on the site. The only exception is represented by ACS08, which shows an amplitude about half of, and flatter in shape than, those obtained from the other sites. Some researchers found that the topographic slope, besides altering the peaks of the horizontal seismic ground acceleration, generates a parasitic vertical acceleration that has to be superimposed on the incoming seismic excitation (Bouckovalas and Papadimitriou 2005; Massa et al. 2014). Therefore, the vertical component's amplification could be because of the topographic aggravation that would be superimposed on the stratigraphic effects on the horizontal components of the ground motion. This particular topographic effect has an effect on the alternating amplification phenomena (amplify or mitigate) of the ground motion near the edge (Bouckovalas and Papadimitriou 2005). It is worth mentioning that the ACS08 station is located precisely on the border of the terrace of Cagnano. The SSRs at this site suffer a reduced amplification with respect to the other site of Cagnano (ACS03) both for horizontal and vertical motions. Furthermore, the clear peak at around 3 Hz is characterized by polarization in the WE direction (HVSr map for noise and moderate earthquakes in Fig. 5) that is almost perpendicular to the main elongation of the ridge (i.e., NNE–SSW). It is worth emphasizing that the correlation between the contained vertical and horizontal amplification effects at the ACS08 site (with respect to the ACS03 site) and topographic arrangement need further specific analyses.

In accordance with previous results and in agreement with the literature, the HVSr allows the recognition of the resonance frequency with more accuracy, although it does not provide comprehensive information regarding the amplification factors or the higher modes (cf. Perron et al. 2018). Additionally, as already shown by the authors previously cited, SSR and HVSr define similar values up to almost the resonance frequency. Contrariwise, the SSR generally overestimates the amplitudes around the peaks with respect to the HVSr. By analyzing the SSR obtained by the earthquakes, values close to unitary amplification are shown to be up to about 1.5 Hz. Instead, the first peaks are in the range between 2 Hz and 7 Hz and probably exist due to the site effects. We can assume that the stations 'see' the same source and path. This is generally accepted if the hypocentral distance (tens of kilometers) is significantly greater than the site-to-reference distance (a few hundred meters) (Borcherdt 1970; Perron et al. 2018).

By interpreting the results with reference to the available information about the geological setting (cf. Fig. 2) and geotechnical properties, some considerations can be drawn. The site ACS02 lies at the valley bottom above a thin layer of travertine with a thickness of approximately 10 m corresponding to the natural frequency at about 19 Hz (obtained by $f = V_s/4H$, with H thickness of the layer and assuming $V_s = 770$ m/s as suggested by Stangoni 2013); this layer

produces a seismic impedance contrast with the base formation. Similarly, the spectral peak at ACS01 corresponds to a greater thickness of the same layer (about 45 m), assuming it to be homogeneous. Hence, no variation of V_s exists with the depth. Instead, the sites ACS03 and ACS08 display (below 10 Hz) amplification in a wider frequency range, which probably contains the effects due to the two impedance contrasts: that between the Miocene formation and the travertine, and the other between the latter layer and the alluvial deposit. In fact, the first peak at frequency around 3 Hz should correspond to a thicker layer of travertine (about 60 m), whereas, the other peaks at frequency between 5 and 7 Hz (which are clearly identifiable in the transverse components in Fig. 6), are compatible with a thick alluvial deposit approximately 10–15 m (considering V_s to be about 300 m/s as suggested by Stangoni 2013). Nevertheless, both impedance ratios were about 3, which should correspond to the maximum of the amplification function in the hypothesis of an elastic homogeneous layer on a deformable substrate (Roesset, 1970). Contrariwise, this value is lower than the amplification provided by the experimental ratios. Finally, SSR at the site on the left slope of the valley reports a peak at 6 Hz. This is probably due to the alluvial deposit lying directly on the Miocene formation, thus the impedance ratio should be significantly greater (>5), according to the available information provided by Rosmarini (2011). The same peak cannot be clearly detected by the HVSr, because the site amplification is observed on all the components (horizontal and vertical) around the same frequency (cf. Fig. 6). The amplitude of the experimental ratios (especially those of the SSR) are appreciably higher than the maximum amplification factor expected from ideal subsoil (i.e. elastic homogeneous layer on deformable substrate), suggesting that the seismic local response is significantly affected by amplification phenomena related both to the topographic arrangement and the stratigraphic geometry.

Site effects on the energy content

Arias intensity (I_A) is one of the widely used parameters in engineering applications to incorporate the amplitude, frequency content and duration of ground motion (Travasarou et al. 2003; Stafford et al. 2009). The parameter is defined as the cumulative energy per unit weight absorbed by an infinite set of undamped single-degree-of-freedom oscillators at the end of an earthquake (Arias 1970). Thus, I_A in the x -direction is expressed as follows:

$$I_{A,x} = \frac{\pi}{2g} \int_0^{T_d} a_x^2(t) dt \quad (1)$$

where $a_x(t)$ is the acceleration time history in the x -direction, g is the acceleration of gravity and T_d is the total duration of

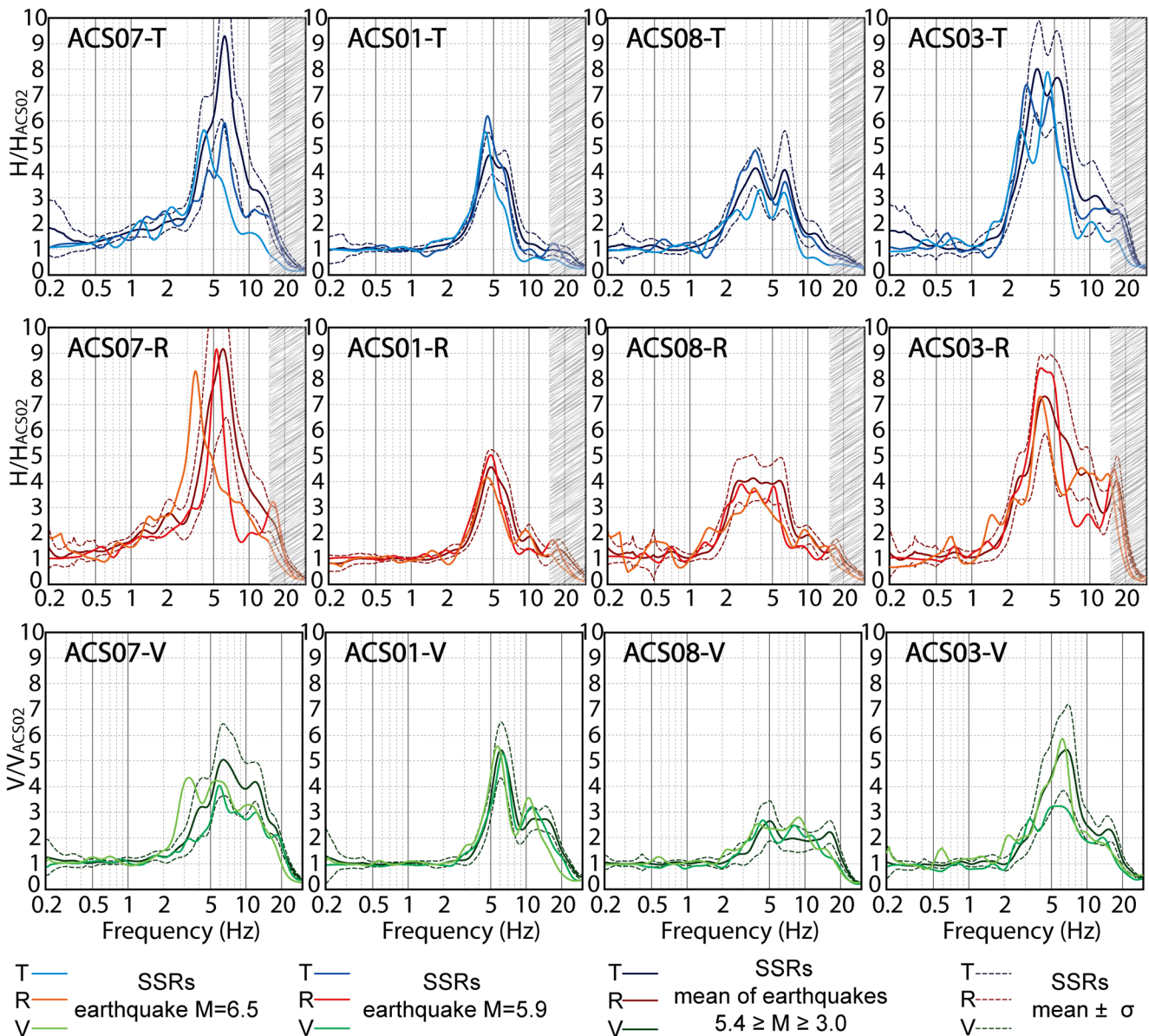


Fig. 6 Standard spectral ratios as horizontal-to-horizontal (vertical-to-vertical) ratio of the Fourier spectra (those at the ACS02 station were used as reference), with comparison among the mean of 30 earthquakes ($5.4 \geq M \geq 3.0$), Mw 5.9 Visso earthquake and Mw 6.5 Norcia earthquake. The horizontal motions for the earthquakes were rotated using

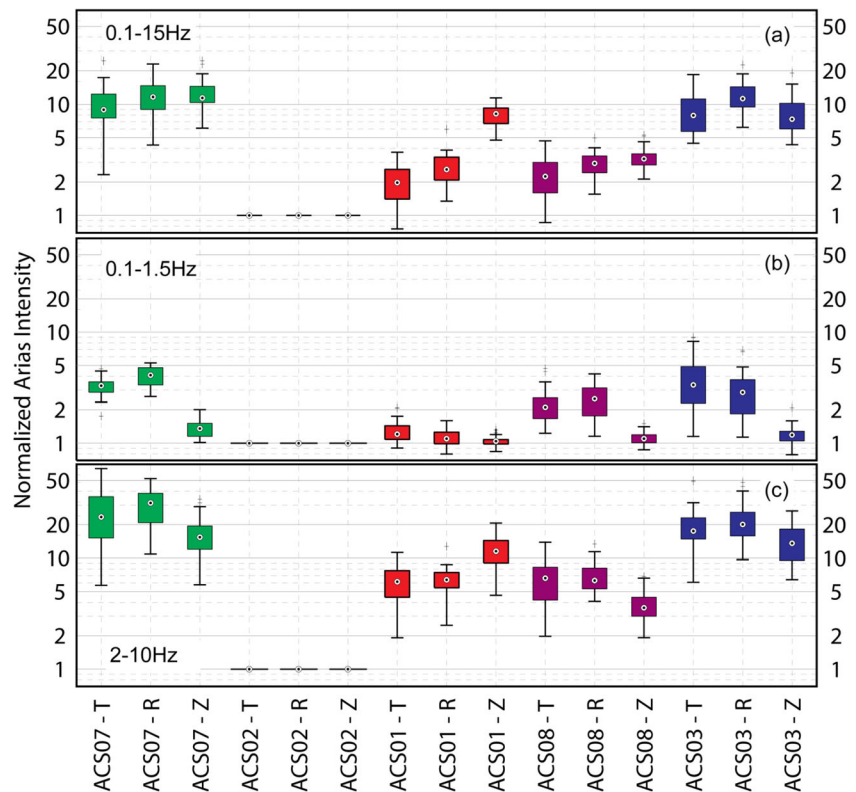
the site-to-epicenter azimuth in Table 2, obtaining transverse (upper row) and radial (middle row) components. The ratios of the vertical components are also drawn (lower row). The ratios are not reliable above 15 Hz

ground motion. I_A is an effective indicator of the potential destructiveness of an earthquake in the form of seismic slope failure (Jibson et al. 2000; Gaudio et al. 2003; Bray and Travasarou 2007; Chousianitis et al. 2014), structural damage (Cabanas et al. 1997; Danciu and Tselentis 2007; Campbell and Bozorgnia 2012; Costanzo 2018) and soil liquefaction (Kayen and Mitchell 1997).

To analyze the site conditions, considering the variation of the ground motion in terms of amplification, frequency content and duration simultaneously, we computed a normalized Arias intensity ($I_{A,N}$) as the ratio between I_A at a site and that at the reference

site (ACS02) for each earthquake and component (Fig. 7). The values of $I_{A,N}$ were obtained by acceleration time histories filtered with an acausal band-pass Butterworth filter of the 4th order in three different bands: 0.1–15 Hz to analyze a wide frequency content; 0.1–1.5 Hz, characterized by negligible amplification; 2–10 Hz, with the primary amplification effects. In Fig. 7, $I_{A,N}$ obtained by 32 earthquakes (Table 2) is plotted in a logarithmic scale, thereby identifying the range between the 25th and 75th percentile (colored box) and median value (white circle). To be more comprehensive, the minimum and maximum values are also reported (bold horizontal lines) in the same figure. By

Fig. 7 Arias intensities at the sites normalized with respect to that of the ACS02 reference station. The Arias intensities were obtained by acceleration time histories filtered with acausal bandpass Butterworth filter of 4th order. Three analogous graphs were produced varying the band of the filter: 0.1–15 Hz (a), 0.1–1.5 Hz (b) and 2–10 Hz (c). The colored box represents the confidence (between 25th and 75th percentile) and the circle is the median, whereas the bold lines are the range between maximum and minimum. The normalized Arias intensities are reported for each site and component (transverse - T, radial - R, and vertical - Z)



analyzing $I_{A,N}$ obtained on the entire frequency range (Fig. 7a), we again note the greater amplification at the sites characterized by significant thickness of soft soil (ACS03 and ACS07), whereas the increase in the energy content is lower where the travertine is almost outcropping (ACS01). A particular case is represented by ACS08, where energy contents from the horizontal components are comparable with those at ACS01, despite vertical components consistently being substantially lower. The vertical components generally produce values of the ratio comparable with those obtained through the horizontal motions at the same site. However, $I_{A,N}$ by vertical components assumes an unexpected value only at the town center of Acquasanta Terme, which is equal to approximately four times those by horizontal ones.

By applying the band-pass filter to the recordings at low frequencies (0.1–1.5 Hz in Fig. 7b), the ratios are always lower than those shown in the previous case with values consistently below 5. Moreover, for all components of the motion recorded at the ACS01 site and for all the vertical components, the amplification effects are negligible (ratio close to one). Instead, using a band-pass filter in the range of 2–10 Hz, a median value 15 and 20 times higher than that at the valley bottom is achieved at the ACS03 and ACS07 sites, respectively. On the other hand, $I_{A,N}$ obtained by vertical components is practically comparable among all sites except ACS08, which was already explained through the analysis of the standard spectral ratios and attributed to the topographic position.

Comparison between experimental data and prediction models

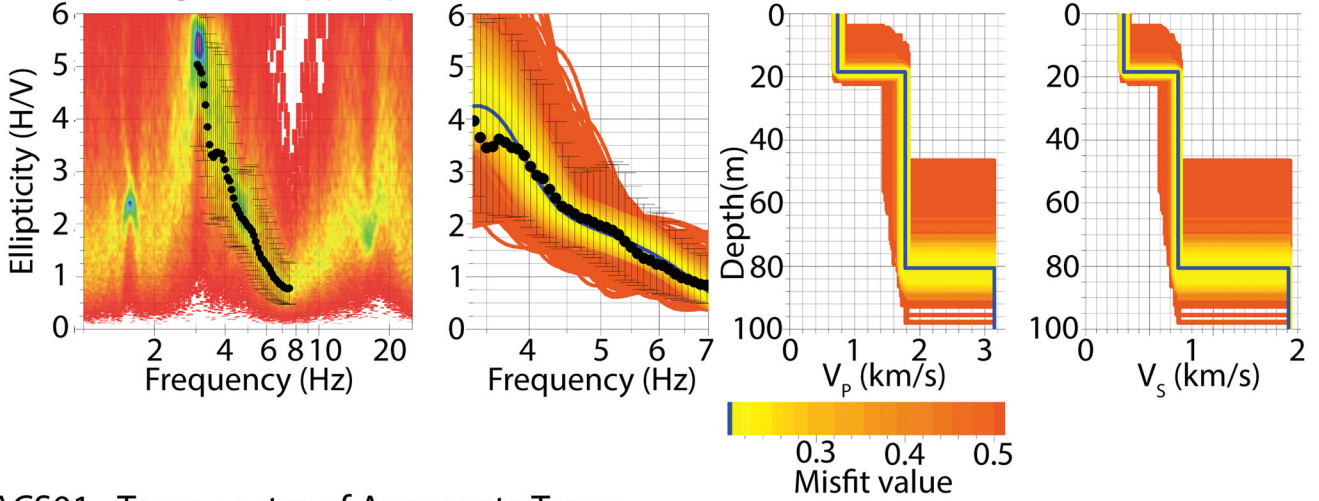
Simplified 1D subsoil models were required for the analysis of the overall match between the experimental spectral accelerations and those of the prediction models. For this purpose, information pertaining to wave velocity profiles were obtained by combining previous geophysical surveys (cf. Stangoni 2013; GEA 2007) that focused on the drafting of technical designs, and the inversion of the ellipticity curves was obtained by HVNSR. The comparisons are limited to sites along the right flank of the river where the local geological setting is better known and the settlements more densely inhabited i.e., at the thermal area at the valley bottom (ACS02), town center (ACS01) and upper part of the Cagnano village (ACS03).

Several researchers consider the H/V curve obtained by ambient vibration as a comprehensive measurement of the

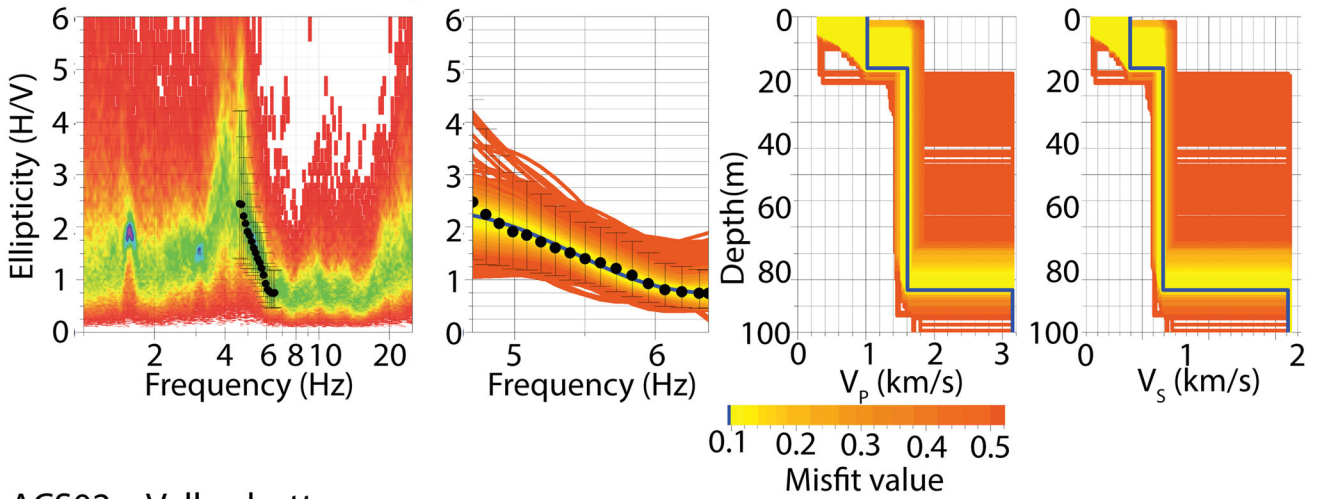
Table 3 Parameter ranges used in the inversions; the velocity decrease is not allowed with depth

	shear wave velocity V_s (m/s)	thickness h (m)	Poisson's ratio ν
Top layer	100–500	1–30	0.35
Travertine layer	600–900	1–80	0.35
Marly unit – Half-space	1900		0.20

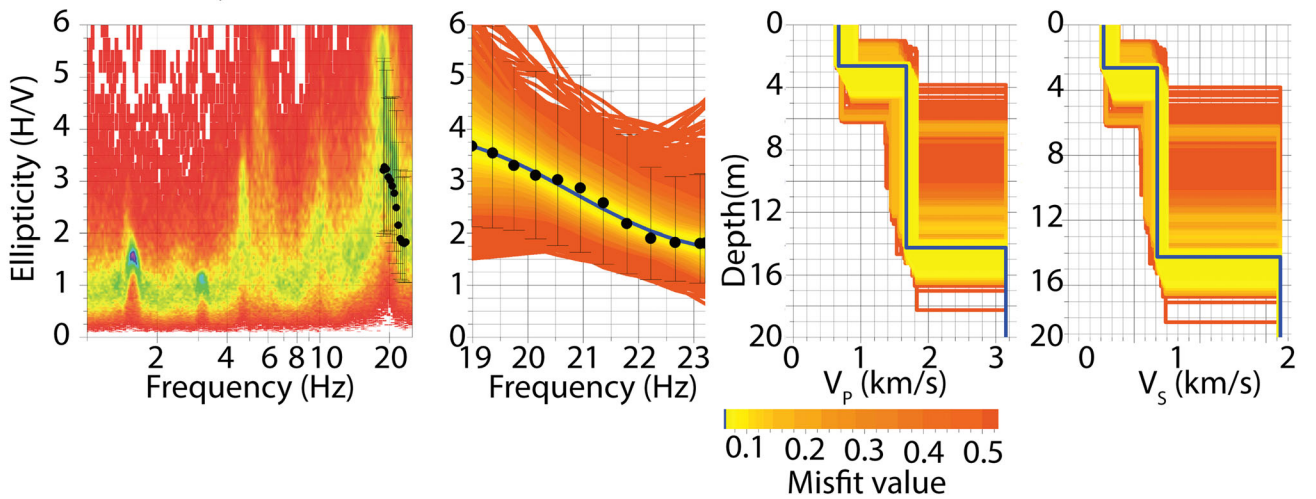
ACS03 - Cagnano upper part



ACS01 - Town centre of Acqusanta Terme



ACS02 - Valley bottom



◀ **Fig. 8** HVTFA curves for fundamental mode (panels of the 1st column). The colored background image is a 2-D histogram of the distribution of ellipticity values calculated at a given frequency, selecting the 5 largest maxima per minute in the time-frequency decomposition. The black dots with error bars are the right flank of the fundamental mode ellipticity curve selected from these data for the inversion. In addition, the results of the inversion technique in terms of fitting values to the data (panels of the 2nd column) and P and S wave velocity profiles (panels of the 3rd and 4th column, respectively) are reported. The best-fit subsoil models (with minimum misfit values) are represented by blue lines. The analyses were performed for the three more densely built areas along the Tronto Valley section (ACS02, ACS01, ACS03 sites)

frequency-dependent Rayleigh wave ellipticity (cf. Fäh et al. 2001; Bonnefoy-Claudet et al. 2006), which can be used in an inversion process to obtain information regarding the wave velocity profile along the subsoil. Hobiger et al. (2013) investigated the part of the Rayleigh wave ellipticity curve that contains relevant information on soil structure and is useful in the inversion process. They found that the right flank of the ellipticity peak, along with the peak frequency, was the most informative part (cf. Fäh et al. 2001), especially for curves with a strong singularity. In this work, the HVTFA (H/V using Time-frequency analysis) method implemented in the GEOPSY software was adopted (SESAME 2004). The method uses a continuous wavelet transform based on the modified Morlet wavelets (Lardies and Gouttebroze 2002) and requires two inputs—the Morlet wavelet parameter that controls the wavelet width in the spectral domain and the number of maxima on the vertical component. Based on the study reported by Fäh et al. (2009), we have selected 8 as the Morlet wavelet parameter and 5 as the maxima per minute. In the inversion process, we introduced a priori ranges to the parameter space. However, the assumptions were based on geological knowledge and the results obtained by previous geophysical surveys in the area. By analyzing the sites along the right flank of the Tronto River, we assumed the presence of only two layers over the half-space—a top layer of alluvial deposits (or altered material) and an intermediate layer of the travertine. The marly unit beneath the travertine was set as a half-space; the latter formation of the Miocene marls is characterized by shear wave velocity (V_S) of approximately 1900 m/s, as obtained by the refraction seismic surveys conducted near the town center of Acquasanta Terme for the parking design (GEA 2007). Additionally, a V_S of 770 m/s was estimated for the travertine through another refraction seismic survey (Stangoni 2013) performed in the Cagnano village at a distance of approximately 100 m from the ACS03 site. Moreover, the same survey evaluated a 10 m thick alluvial deposit with a V_S of about 300 m/s overlapping the travertine. In the inversion process, the layer indicated as conglomerates in the geological section sketched by Boni and Colacicchi (1966) (cf. Fig. 2) has not been considered because this was not identified by the available geological studies in the area. In particular, these studies report the

findings of some drillings and show how travertine is directly situated on the Miocene marl formation (Lanzi and Cavanazza 1993; Prezzavento 2007). To simulate the fundamental mode and derive the velocity profiles of the subsoil, only the right flank of the ellipticity peak was used in the inversion process through an improved neighborhood algorithm (Wathelet 2008). The variation of the parameters had been allowed in the ranges reported in Table 3 during the processing by assuming a uniform behavior among all layers.

The left panels in Fig. 8 show the HVTFA results—the 2D histograms of the distribution of the ellipticity values calculated at a given frequency—and also the right flank related to the ellipticity peak. The figures show the shift of the peak from 19 Hz to approximately 3 Hz moving from the valley bottom (ACS02) to the site at higher altitude (ACS03). The other three panels on each row of Fig. 8 display the results of inversion processing, i.e. the fit along the ellipticity target curve and those obtained from the visited models, the velocity profiles of the compression waves (V_P) and shear waves (V_S), respectively, from left to right. During the inversion process, the minimum misfit found in any case was lower than 0.21. The velocity profiles indicate some variability of the thicknesses and velocities related to the top layers. Contrariwise, the velocities of the travertine layer calculated for the three sites seem comparable, since we found V_S between 790 m/s and 840 m/s. Moreover, the velocities are slightly higher than 770 m/s measured in the previous surveys (cf. Stangoni 2013). Instead, the thickness of the travertine layer increases from 12 m for the site at the valley bottom to 42 m beneath the town center of Acquasanta Terme and goes above 60 m in Cagnano village.

The velocity profiles of the shear waves are numerically summarized in Table 4. In the same table, $V_{S,30}$ is calculated using Eq. (2) and the site classification according to the European technical code is also reported.

$$V_{S,30} = \frac{30}{\sum_{i=1}^N \frac{h_i}{V_{S,i}}} \quad (2)$$

In Eq. (2), h_i and $V_{S,i}$ are, respectively, the thickness and shear wave velocity of the i^{th} layer of the N layers encountered up to a depth of 30 m.

The elastic response spectra were calculated considering 5% damping through recordings of the Mw 6.5 Norcia earthquake and Mw 5.9 Visso earthquake to analyze the seismic actions related to the two events. The results are recorded in the upper and lower row of Fig. 9, respectively. It should be noted that some features in the response spectra were observed previously in the FAS plots (Fig. 3). The pronounced amplification on the ground motion components can be observed with respect to the reference site ACS02 between 0.1 and 0.5 s, depending predominantly on the site and vice versa. The small difference in the pseudo-spectral acceleration

Table 4 Results obtained by the inversion process

Site	ACS02		ACS01		ACS03	
	Vs (m/s)	Thickness (m)	Vs (m/s)	Thickness (m)	Vs (m/s)	Thickness (m)
Top layer	325	2.50	495	10	363	18
Travertine	810	12	790	42	840	63
Half-space	1900	–	1900	–	1900	–
VS,30 (m/s)	978		659		470	
Ground type by EC8	A		B		B	

(PSA) at periods greater than 1 s emphasized the limited effects for the local conditions above this period. It is worth mentioning that the spectra show peaks above 1 g at all the sites in the case of the Norcia earthquake and greater than about 0.3 g for the Visso earthquake.

In Fig. 9, the response spectra were also superimposed on the predictions obtained using two GMPEs that are based on the earthquakes recorded in the Italian region and worldwide. The median values provided by GMPEs were calculated using the Joyner-Boore distance (R_{jb} , Joyner and Boore 1981) of

9.7 km (from site to source) and through the $V_{S,30}$ reported in Table 4, using both B&A08 (Boore and Atkinson 2008) modified using the adjustment proposed by Scasserra et al. (2009) (which were derived using data from Italian earthquakes) and B&all11 (Bindi et al. 2011) relationships (black and green solid lines in Fig. 9 respectively); the confidence intervals (as median \pm one standard deviation) are indicated with dashed lines. The graphs related to the B&all11 show significantly high total standard deviations. Contrariwise, the variability is restrained for B&A08. The large variability in the

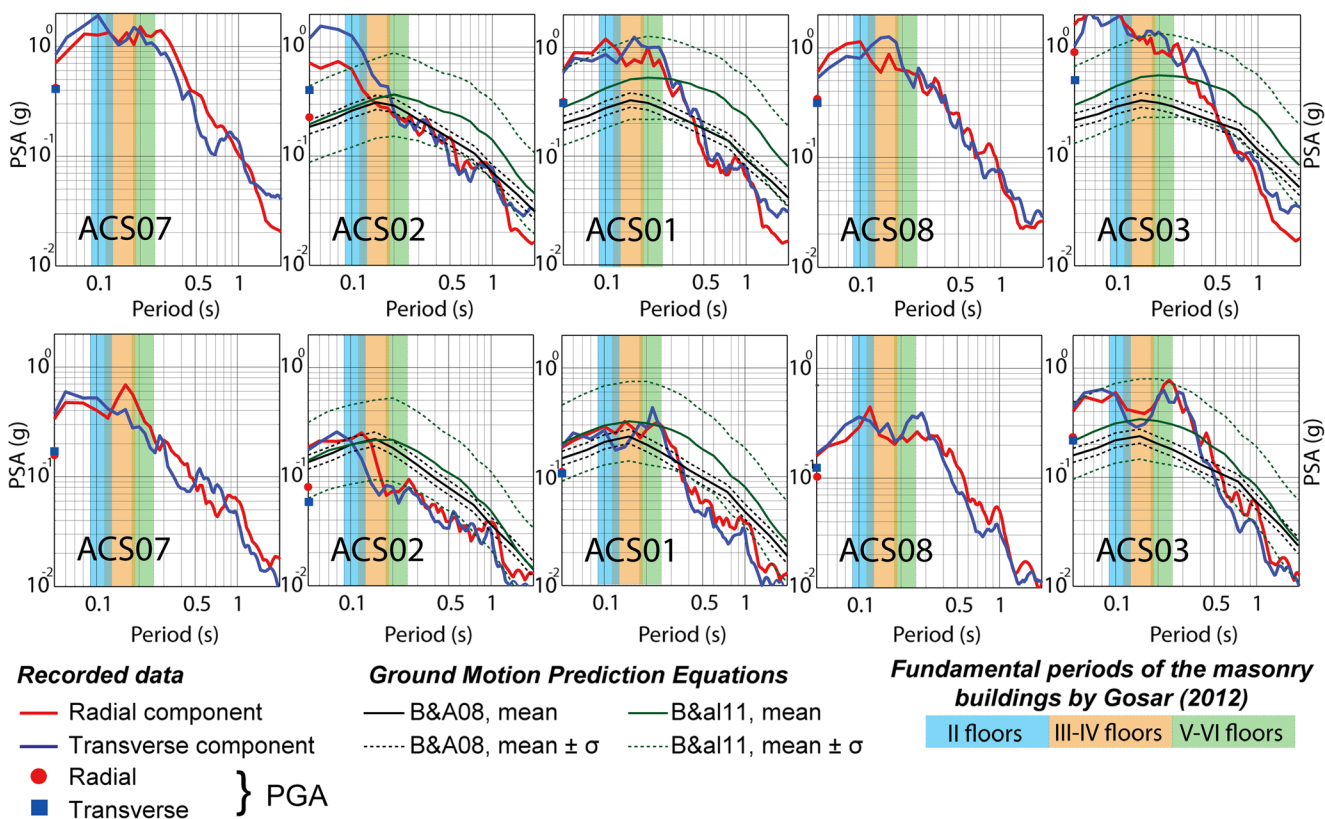


Fig. 9 Response spectra with 5% damping obtained by horizontal motions at the different sites (blue lines for the transverse components and red lines for the radial ones), both for the Mw 6.5 Norcia earthquake (upper panel) and the Mw 5.9 Visso earthquake (lower panel). In addition, the Peak Ground Accelerations (PGA) are indicated. The pseudo-accelerations are compared with those obtained by two Ground Motion Prediction Equations (GMPE) [B&A08: Boore and Atkinson (2008),

modified using the Scasserra et al. (2009) distance indications; B&all11: Bindi et al. (2011)]. The mean values (solid lines) and the statistical dispersion (dashed lines) are indicated as functions of the $V_{S,30}$ and the R_{jb} distance (Joyner and Boore 1981). Moreover, the fundamental frequency (\pm one standard deviation) of masonry structures given by Gosar (2012) are reported with reference to the number of floors

ground shaking parameters is probably related to the regional dataset that contains mostly small and moderate magnitude events (Douglas 2007; Akkar and Cagnan 2010). By comparing experimental and predicted spectra, it is observed that the spectral shape of the Norcia earthquake is quite different from the predictions; the experimental spectral accelerations are evidently greater than the median predictions at low periods (< 0.5 s and < 0.3 s for B&A08 and B&A11, respectively). Contrariwise, at high periods the GMPEs appear to be precautionary. With reference to the Visso earthquake (Mw 5.9), however, the observed PSAs are more comparable with the median values of the predictions at low periods, with the exception of the ACS03 site. For ACS03, the PSAs observed are placed at the upper bound provided by B&A11. We should not expect the ground motion from the recordings of single earthquakes to be consistently close to the median values from a large global dataset. Nevertheless, it is significant that the spectral accelerations provided by the recordings in many cases greatly exceed the upper bound of the GMPE when the standard deviation is contained (e.g., B&A08), or are placed on this limit with a given large variability (e.g., B&A11). This trend is more significant if the interested period ranges intersect the fundamental periods of vibration related to the masonry structures that were built in proximity to the investigated sites. In Fig. 9, the fundamental periods obtained by Gosar (2012) for residential masonry buildings as a function of the number of floors are indicated as a reference. In particular, the author measured the microtremor inside 66 residential masonry buildings in five Slovenian towns and obtained the fundamental frequencies as a function of their height (or number of floors).

Conclusions

Since September 05, 2016, we recorded severe earthquakes (Mw ≥ 5.9) and aftershocks of the Central Italy seismic sequence that struck the area along Amatrice, Norcia and Visso, and deployed a temporary seismic array along the valley of the Tronto River corresponding to the town of Acquasanta Terme (AP, Marche). The seismic sequence provided several recordings of the earthquakes with variable magnitudes, which allowed us to study the seismic site response. The seismic recordings were with reference to five sites—three along the right flank of the valley, where the main settlements of the town were built—one at the valley bottom, almost in contact with the seismic bedrock and the last one on the other side of valley, close to another small hamlet. The comparison between the recordings obtained from two stronger earthquakes (Mw 6.5 Norcia and Mw 5.9 Visso), thirty aftershocks and the ambient noise revealed significant local effects with amplifications into specific frequency ranges, depending on the site conditions. The natural frequencies

detected by HVSR at the sites going up along the right side of the valley were 19 Hz at the bottom, 4 Hz in the town center of Acquasanta Terme and approximately 3 Hz in the village of Cagnano. The HVSR obtained by recordings at the site—on the left side of the valley—appeared not to show a dominant peak. Moreover, the SSRs (calculated as ratio with respect to the recordings at the valley bottom) clearly define the frequency ranges where the amplifications were detected, highlighting significant local effects at all the investigated sites. In particular, SSR amplitudes around 4 were observed in the town center; values above 8 were encountered near the settlements of Cagnano and San Vito, i.e., the sites at a higher altitude along the right and left flanks of the Tronto River. The observations on the local effects were also confirmed from the normalized Arias intensity. The overall framework outlined by the analysis of the experimental data and the geological information suggests that the experimental natural frequencies are compatible with the local stratigraphic sequence. However the amplifications greater than expected ones—compared to the estimated impedance ratios and an ideal behavior of the subsoil—suggest that the seismic response is affected by significant effects related to the ‘real’ topographic and stratigraphic arrangement.

In agreement with literature, the HVSR allowed us to recognize the first fundamental frequency with more accuracy, with the exception of the ACS07 site, where the vertical amplification seems to hide it. Instead, SSR defines amplitudes significantly higher with respect to those of the HVSR, with values greater than 3 for wider frequency ranges. A particular case is represented by the ACS08 site, where horizontal and vertical SSRs showed more contained amplifications than those obtained for ACS03 (about 200 m away); the causes of this behavior should be investigated more thoroughly.

Finally, the analysis of the response spectra by the recordings of the two stronger earthquakes have shown that the GMPE provided by Boore and Atkinson (2008) is almost always not precautionary for a period lower than 0.35 s, except for the site at the valley bottom. The upper bound values, furthermore, of the spectral acceleration obtained by GMPE provided by Bindi et al. (2011) are lower than (or comparable with) the measured ones in several cases, despite the presence of large total standard deviations of this relationship. It is noteworthy that these unexpectedly high spectral accelerations fall in the range of fundamental periods for masonry buildings, which represent the main historic structures built in the town of Acquasanta Terme and its villages. Thus, the ancient buildings (especially those with more than two floors) and the thermal structures located at the valley bottom have been subjected to smaller spectral accelerations in correspondence with their predominant period, although these were significant during the two strong earthquakes (cf. Fig. 9). Instead, the ground shaking has shown amplification in the engineering frequency range while moving towards the town center, and more at the Cagnano and San Vito villages,

and is especially interesting for ancient buildings. The higher spectral accelerations concurred with the preliminary observations regarding damage following the Amatrice earthquake. Therefore, the rebuilding effort should consider higher seismic requirements for the structures located along the slopes of the valley, especially the ancient ones with more than two floors. Moreover, the ground motion has shown significant differences within relatively small spatial variation. Thus, a microzonation plan (which also includes other hamlets of Acquasanta Terme) and a site-specific study are required for assuring a performance-based design of ancient and recent structures.

Acknowledgements The data used in this study were collected thanks to the collaboration of the whole town of Acquasanta Terme. In particular the local authorities and the Municipality in supporting our researcher and logistic needs. The authors are also grateful to the anonymous reviewers and the Editor-in-Chief Prof. M.G. Culshaw for their thoughtful and constructive reviews of the manuscript. The study has been done thanks to funds provided by the Italian Civil Protection.

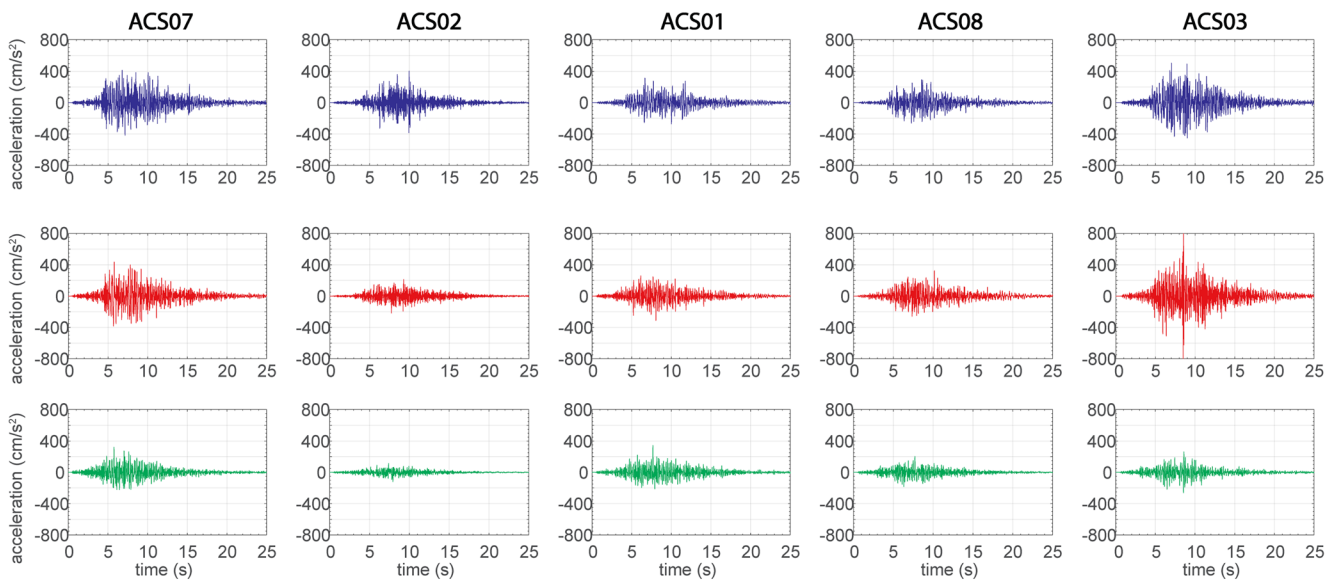
Appendix A

#1 - 2016.X.30 Norcia earthquake Mw=6.5

— Transverse

— Radial

— Vertical



#2 - 2016.X.26 Visso earthquake Mw=5.9

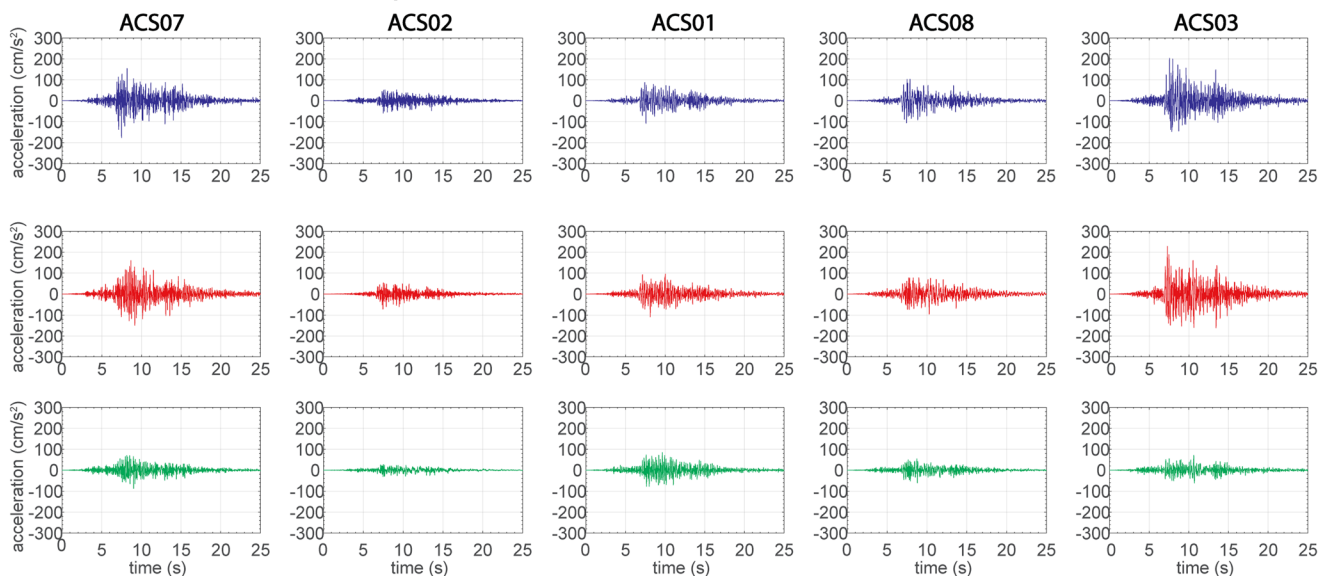


Fig. 10 Acceleration time histories recorded at the sites during the Mw 6.5 Norcia earthquake (upper panel) and Mw 5.9 Visso earthquake (lower panel)

References

- Akkar S, Cagnan Z (2010) A local ground-motion predictive model for Turkey and its comparison with other regional and global ground-motion models. *Bull Seismol Soc Am* 100(6):2978–2995. <https://doi.org/10.1785/0120090367>
- Arias A (1970) A measure of earthquake intensity. In: Hansen RJ (ed) *Seismic Design for Nuclear Power Plants*. MIT Press, Cambridge, pp 438–483
- Bindi D, Pacor F, Luzi L, Puglia R, Massa M, Ameri G, Paolucci R (2011) Ground motion prediction equations derived from the Italian strong motion database. *Bull Earthq Eng* 9(6):1899–1920. <https://doi.org/10.1007/s10518-011-9313-z>
- Boni C, Colacicchi R (1966) I travertini della valle del Tronto [the travertines of the Tronto Valley]. *Mem Soc Geol Ital* 5:315–339
- Bonnefoy-Claudet S, Cornou C, Bard P-Y, Cotton F, Moczo P, Kristek J, Fäh D (2006) H/V ratio: a tool for site effects evaluation. Results from 1-D noise simulations. *Geophys J Int* 167(2):827–837. <https://doi.org/10.1111/j.1365-246X.2006.03154.x>
- Boore DM, Atkinson GM (2008) Ground-motion prediction equations for the average horizontal component of PGA, PGV, and 5%-damped PSA at spectral periods between 0.01 s and 10.0 s. *Earthq. Spectra* 24(1):99–138. <https://doi.org/10.1193/1.2830434>
- Borcherdt RD (1970) Effects of local geology on ground motion near San Francisco Bay. *Bull Seism Soc Am* 60:29–61. <https://doi.org/10.1193/1.2830434>
- Bouckovalas GD, Papadimitriou AG (2005) Numerical evaluation of slope topography effects on seismic ground motion. *Soil Dyn Earthq Eng* 25(7):547–558. <https://doi.org/10.1016/j.soildyn.2004.11.008>
- Bray JD, Travararou T (2007) Simplified procedure for estimating earthquake induced deviatoric slope displacements. *J Geotech Geoenviron Eng* 133(4):381–392. [https://doi.org/10.1061/\(ASCE\)1090-0241\(2007\)133:4\(381\)](https://doi.org/10.1061/(ASCE)1090-0241(2007)133:4(381))
- Cabanas L, Benito B, Herráiz M (1997) An approach to the measurement of the potential structural damage of earthquake ground motion. *Earthq Eng Struct Dynam* 26(1):79–92. [https://doi.org/10.1002/\(SICI\)1096-9845\(199701\)26:1<79::AID-EQE624>3.0.CO;2-Y](https://doi.org/10.1002/(SICI)1096-9845(199701)26:1<79::AID-EQE624>3.0.CO;2-Y)
- Campbell KW, Bozorgnia Y (2012) A comparison of ground motion prediction equations for Arias intensity and cumulative absolute velocity developed using a consistent database and functional form. *Earthquake Spectra* 28(3):931–941. <https://doi.org/10.1193/1.4000067>
- Caserta A, Doumaz F, Costanzo A, Gervasi A, Thorossian W, Falcone S, La Piana C, Minasi M, Buongiorno M (2016) Assessing soil-structure interaction during the 2016 Central Italy seismic sequence (Italy): preliminary results. *Ann Geophys (FT5)*:59. <https://doi.org/10.4401/ag-7250>
- Chousianitis K, Gaudio VD, Kalogeras I, Ganas A (2014) Predictive model of Arias intensity and Newmark displacement for regional scale evaluation of earthquake-induced landslide hazard in Greece. *Soil Dynam Earthq Eng* 65:11–29. <https://doi.org/10.1016/j.soildyn.2014.05.009>
- Costanzo A (2018) Shaking maps based on cumulative absolute velocity and Arias intensity: the cases of the two strongest earthquakes of the 2016–2017 Central Italy seismic sequence. *ISPRS Int J Geo-Inf* 7(7):244. <https://doi.org/10.3390/ijgi7070244>
- Cultrera C, D'Alema E, Amoroso S, Angioni B, Bordoni P, Cantore L, Cara F, Caserta A, Cogliano R, D'Amico M, Di Giulio G, Di Naccio D, Famiani D, Felicetta C, Fodarella A, Lovati S, Luzi L, Massa M, Mercuri A, Milana G, Pacor F, Pischiutta M, Pucillo S, Puglia R, Riccio G, Tarabusi G, Vassallo M, Mascandola C (2016) Site effect studies following the 2016 mww 6.0 Amatrice earthquake (Italy): the Emersito task force activities. *Ann Geophys* 59(FT5). <https://doi.org/10.4401/ag-7189>
- Danciu L, Tselentis GA (2007) Engineering ground-motion parameters attenuation relationships for Greece. *Bull Seismol Soc Am* 97(1B):162–183. <https://doi.org/10.1785/0120050087>
- Douglas J (2007) On the regional dependence of earthquake response spectra. *ISET J Earthq Technol* 44(1):71–99
- Fäh D, Kind F, Giardini D (2001) A theoretical investigation of average H/V ratios. *Geophys J Int* 145:535–549. <https://doi.org/10.1046/j.0956-540x.2001.01406.x>
- Fäh, D., Wathelet, M., Kristekova, M., Havenith, H., Endrun, B., Stamm, G., Poggi, V., Burjanek, J., Cornou, C. (2009) Using ellipticity information for site characterisation. D4, final report EC project number: 026130, NERIES JRA4 “Geotechnical Site Characterisation”, task B2
- Farabollini, P., Gentili, B., Materazzi, M. (2001) Freshwater travertines in the Central Apennine (Italy): Genesis and climatic and neotectonic significance, in *Proceedings, International Conference on Geomorphology 5th*, Tokyo, p. 8–10
- Fiorentino G, Forte A, Pagano E, Sabetta F, Baggio C, Lavorato D, Nuti C, Santini S (2018) Damage patterns in the town of Amatrice after August 24th 2016 Central Italy earthquakes. *Bull Earthq Eng* 16(3):1399–1423. <https://doi.org/10.1007/s10518-017-0254-z>
- Galdenzi S, Cocchioni F, Filippini G, Morichetti L, Scuri S, Selvaggio R, Cocchioni M (2010) The sulfidic thermal caves of Acquasanta Terme (Central Italy). *J Cave Karst Stud* 72(1):43–58. <https://doi.org/10.4311/jcks2008es0056>
- Galli P, Castenetto S, Peronace E (2017) The macroseismic intensity distribution of the 30 October 2016 earthquake in Central Italy (mw 6.6): seismotectonic implications. *Tectonics* 36:2179–2191. <https://doi.org/10.1002/2017TTC004583>
- Gaudio VD, Pierri P, Wasowski J (2003) An approach to time probabilistic evaluation of seismically induced landslide hazard. *Bull Seismol Soc Am* 93(2):557–569. <https://doi.org/10.1785/0120020016>
- GEA (2007) Indagine geofisica sul terreno di fondazione interessato dal progetto di un parcheggio pubblico da realizzarsi nel Comune di Acquasanta Terme. Report of the geophysical survey
- Gosar A (2012) Determination of masonry building fundamental frequencies in five Slovenian towns by microtremor excitation and implications for seismic risk assessment. *Nat Hazards* 62(3):1059–1079. <https://doi.org/10.1007/s11069-012-0138-0>
- Haghshenas E, Bard PY, Theodoulidis N, SESAME WP04 Team (2008) Empirical evaluation of microtremor H/V spectral ratio. *Bull Earthq Eng* 6(1):75–108. <https://doi.org/10.1007/s10518-007-9058-x>
- Hobiger M, Cornou C, Wathelet M, Di Giulio G, Knapmeyer-Endrun B, Renalier F, Bard PY, Savvaidis A, Hailemikael S, Le Bihan N, Ohmberger M, Theodoulidis N (2013) Ground structure imaging by inversions of Rayleigh wave ellipticity: sensitivity analysis and application to European strong-motion sites. *Geophys J Int* 192(1):207–229. <https://doi.org/10.1093/gji/ggs005>
- Jibson RW, Harp EL, Michael JA (2000) A method for producing digital probabilistic seismic landslide hazard maps. *Eng Geol* 58(3–4):271–289. [https://doi.org/10.1016/S0013-7952\(00\)00039-9](https://doi.org/10.1016/S0013-7952(00)00039-9)
- Joyner WB, Boore DM (1981) Peak horizontal acceleration and velocity from strong-motion records including the records from the 1979 Imperial Valley, California, earthquake. *Bull Seism Soc Am* 71:2011–2038
- Kayen RE, Mitchell JK (1997) Assessment of liquefaction potential during earthquakes by Arias intensity. *J Geotech Geoenviron Eng* 123(12):1162–1174. [https://doi.org/10.1061/\(ASCE\)1090-0241\(1997\)123:12\(1162\)](https://doi.org/10.1061/(ASCE)1090-0241(1997)123:12(1162))
- Konno K, Ohmachi T (1998) Ground-motion characteristics estimated from spectral ratio between horizontal and vertical components of microtremor. *Bull Seismol Soc Am* 88(1):228–241
- Lanzi, U., Cavanazza, F. (1993) Relazione idrogeologica volta ad illustrare gli aspetti caratterizzanti la falda acquifera del “Pozzo 2”

- in territorio del Comune di Acquasanta Terme. Report of the geological study
- Lardies J, Gouttebroze S (2002) Identification of modal parameters using the wavelet transform. *Int J Mech Sci* 44:2263–2283. [https://doi.org/10.1016/S0020-7403\(02\)00175-3](https://doi.org/10.1016/S0020-7403(02)00175-3)
- Laurenzano G, Barnaba C, Romano MA et al (2018) The Central Italy 2016–2017 seismic sequence: site response analysis based on seismological data in the Arquata del Tronto–Montegallo municipalities. *Bull Earthq Eng*. <https://doi.org/10.1007/s10518-018-0355-3>
- Lermo J, Chávez-García FJ (1993) Site effect evaluation using spectral ratios with only one station. *Bull Seismol Soc Am* 83(5):1574–1594
- Luzi L, D'Amico M, Massa M, Puglia R (2018) Site effects observed in the Norcia intermountain basin (Central Italy) exploiting a 20-year monitoring. *Bull Earthq Eng*. <https://doi.org/10.1007/s10518-018-0444-3>
- Masi A, Santarsiero G, Chiauzzi L, Gallipoli MR, Piscitelli S, Vignola L, Bellanova J, Calamita G, Perrone A, Lizza C, Grimaz S (2016) Different damage observed in the villages of Pescara del Tronto and Vezzano after the M6.0 august 24, 2016 Central Italy earthquake and site effects analysis. *Ann Geophys* 59(FT5). <https://doi.org/10.4401/ag-7271>
- Masi A, Chiauzzi L, Santarsiero G, Manfredi V, Biondi S, Spacone E, Del Gaudio C, Ricci P, Manfredi G, Verderame GM (2017) Seismic response of RC buildings during the mw 6.0 august 24 2016 Central Italy earthquake: the Amatrice case study. *Bull Earthq Eng*. <https://doi.org/10.1007/s10518-017-0277-5>
- Massa M, Barani S, Lovati S (2014) Overview of topographic effects based on experimental observations: meaning, causes and possible interpretations. *Geophys J Int* 197(3):1537–1550. <https://doi.org/10.1093/gji/ggt341>
- Michele M, Di Stefano R, Chiaraluce L, Cattaneo M, De Gori P, Monachesi G, Latorre D, Marzorati S, Valoroso L, Ladina C, Chiarabba C, Luciani V, Fares M (2016) The Amatrice 2016 seismic sequence: a preliminary look at the mainshock and aftershocks distribution. *Ann Geophys* 59(FT5). <https://doi.org/10.4401/ag-7227>
- Nakamura, Y. (2000) Clear identification of fundamental idea of Nakamura's technique and its applications, in Proceedings of the 12th World Conference on Earthquake Engineering, Auckland
- Nanometrics Inc. (2018a). CENTAUR technical specifications. Nanometrics, Inc., Kanata, Ontario, Canada, available on line: <https://www.nanometrics.ca/products/instrumentation/centaur-digital-recorder>. (accessed on September 9, 2018)
- Nanometrics Inc. (2018b). TRILLIUM COMPACT technical specifications. Nanometrics, Inc., Kanata, Ontario, Canada, available online: <https://www.nanometrics.ca/products/instrumentation/trillium-compact-seismometers>. (accessed on September 9, 2018)
- Nanometrics Inc. (2018c). TITAN accelerometer technical specifications. Nanometrics, Inc., Kanata, Ontario, Canada, available on line: <https://www.nanometrics.ca/products/instrumentation/titan-accelerometers>. (accessed on September 9, 2018)
- Perron V, Gélis C, Froment B, Hollender F, Bard PY, Cultrera G, Cushing EM (2018) Can broad-band earthquake site responses be predicted by the ambient noise spectral ratio? Insight from observations at two sedimentary basins. *Geophys J Int* 215(2):1442–1454. <https://doi.org/10.1093/gji/ggy355>
- Pilz M, Parolai S (2009) Norcia basin (Italy) temporary seismic network. GFZ Data Service. <https://doi.org/10.14470/8u7554472182>
- Prezzavento R. (2007) Rapporto geologico con indicazioni geotecniche relativo al progetto per il completamento ed adeguamento dell'ascensore pubblico e parcheggi del capoluogo nel Comune di Acquasanta Terme. *Report of the geological study*
- Roeset J. (1970) Fundamentals of soil amplification. Seismic Design for Nuclear Power Plants. Ed. R.J. Hansen. The M.I.T. Press
- Rosamarini F. (2011) Realizzazione autorimessa interrata e opera interna. *Report of the geological study*
- Scasserra G, Stewart JP, Bazzurro P, Lanzo G, Mollaioli F (2009) A comparison of NGA ground-motion prediction equations to Italian data. *Bull Seismol Soc Am* 99(5):2961–2978. <https://doi.org/10.1785/0120080133>
- SESAME (2004) Guidelines for the implementation of the H/V spectral ratio technique on ambient vibrations measurements, processing and interpretation. SESAME European research project. WP12 – Deliverable D23.12. <http://sesame-fp5.obs.ujf-grenoble.fr/index.htm>
- Stafford PJ, Berrill JB, Pettinga JR (2009) New predictive equations for Arias intensity from crustal earthquakes in New Zealand. *J Seismol* 13(1):31–52. <https://doi.org/10.1007/s10950-008-9114-2>
- Stangoni, S., (2013) Progetto per la realizzazione di un adeguamento su fabbricato di civile abitazione in Frazione Cagnano. Report of the geological study
- Travasariou T, Bray JD, Abrahamson NA (2003) Empirical attenuation relationship for Arias intensity. *Earthq Eng Struct Dynam* 32(7): 1133–1155. <https://doi.org/10.1002/eqe.270>
- Wathelet M (2008) An improved neighborhood algorithm: parameter conditions and dynamic scaling. *Geophys Res Lett* 35(9):L09301. <https://doi.org/10.1029/2008GL033256>